Vertical Nb_2O_5 Micro-Petal Array Photoelectrochemical Deep-UV Photodetectors Towards Underwater Weak-Light Photodetection

Junxin Zhou, Yuan Zhang, Xinyu Gao, Zhitao Shao, Ruyu Sun, Wenhui Li, Xinghan Li, Jiaming Liu, Wei Feng*

College of Chemistry, Chemical Engineering and Resource Utilization, Northeast Forestry University, Harbin, 150040, China

Email: wfeng@nefu.edu.cn

The preparation of the KNb_3O_8 precursor

The preparation of KNb_3O_8 was achieved via a hydrothermal method according to previous work. (*Journal of Alloys and Compounds*, 2015, *627*, 117–122) A 3 M KOH solution (30 mL) was prepared, and 1 g of Nb_2O_5 powder was added and stirred thoroughly using a magnetic stirrer. The mixture was then transferred to a hydrothermal synthesis reactor and heated at 230 °C for 2 h. After cooling to room temperature, HCl was added dropwise to the solution in a fume hood until the pH reached 7 and a white precipitate formed. The precipitate was separated using a centrifuge and washed three times with deionized water. It was then dried in an oven at 60 °C overnight. Finally, the dried solid was ground into fine particles and further dried at 100 °C for 2 h to obtain KNb_3O_8 powder.

The preparation of simulated seawater

6.684 g of NaCl, 0.050 g of $NaHCO_3$, 0.873 g of Na_2SO_4, 0.181 g of KCl, 1.213 g of $MgCl_2 \cdot H_2O$, and 0.813 g of $CaCl_2$ were accurately weighed using an electronic balance. These were added to a beaker containing 250 mL of deionized water and stirred vigorously on a magnetic stirrer for 30 min. The solution was then sealed and stored in a dark place for later use.

The preparation of the Nb_2O_5 microcrystals (MCs)-based PEC PDs

2 mg of PVDF and 20 mg of Nb_2O_5 were dissolved in 10 mL of DMF to form a Nb_2O_5 solution with a concentration of 2 mg mL^{-1} for drop-casting. A volume of 33 μL of this solution was evenly dropped onto an FTO substrate with an area controlled at 1 cm^2, and the substrate was placed in a 60 °C oven until the solvent evaporated. This process was repeated six times, resulting in a total drop-cast volume of 200 μL, to obtain Nb_2O_5 MCs on the FTO glass.

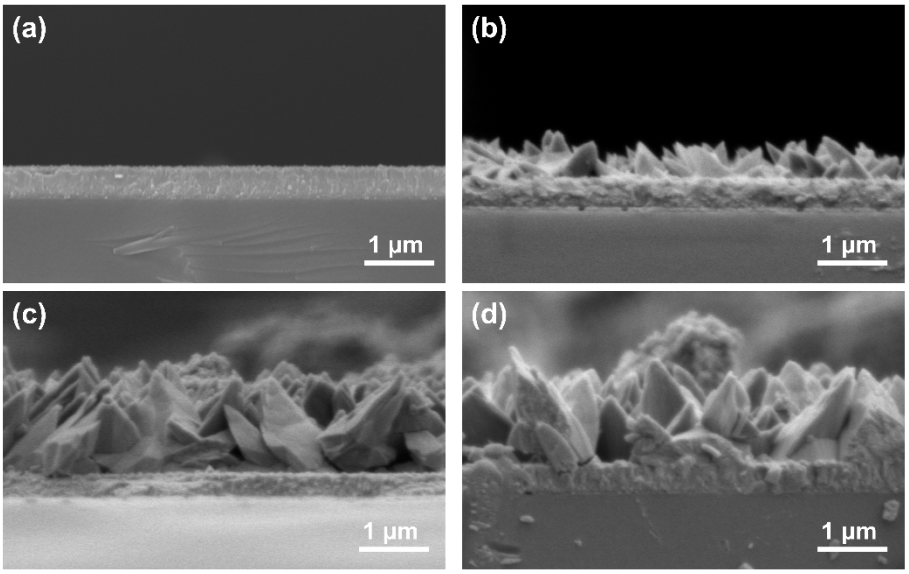

Figure S1. Cross-view SEM images of a) pure FTO glass, b) 1 h, c) 2 h, and d) 3 h-Nb_2O_5 samples.

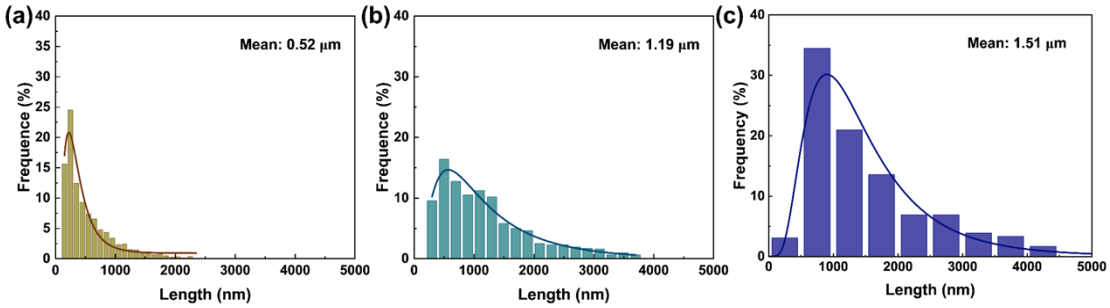

Figure S2. Length distribution diagrams of a) 1 h, b) 2 h, and c) 3 h-Nb_2O_5 samples.

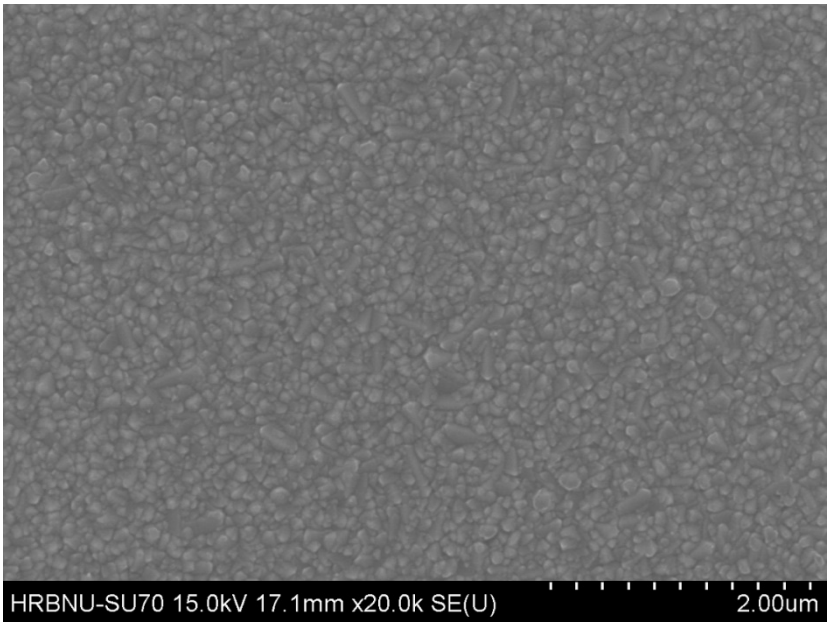

Figure S3. Top-view SEM image of pure FTO substrate.

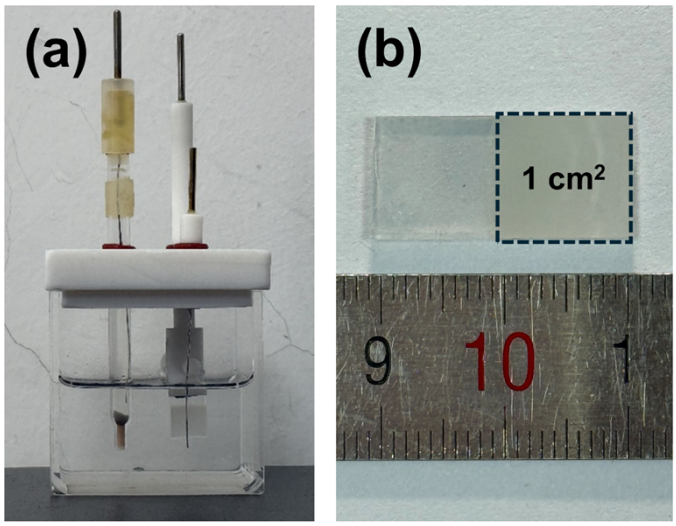

Figure S4. Optical images of a) the three-electrode system and b) the working electrode.

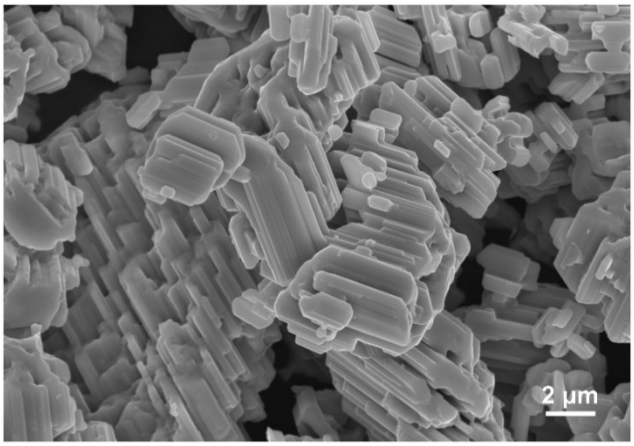

Figure S5. SEM image of Nb_2O_5 MCs powder.

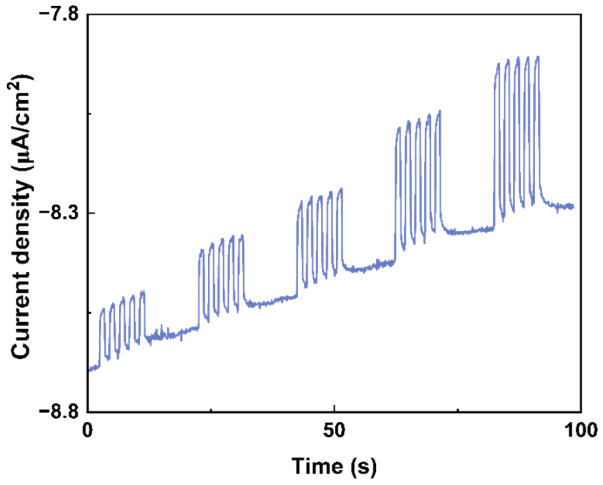

Figure S6. *J*-t curve of Nb_2O_5 MC PEC PDs under 254 nm irradiation with different power intensities.

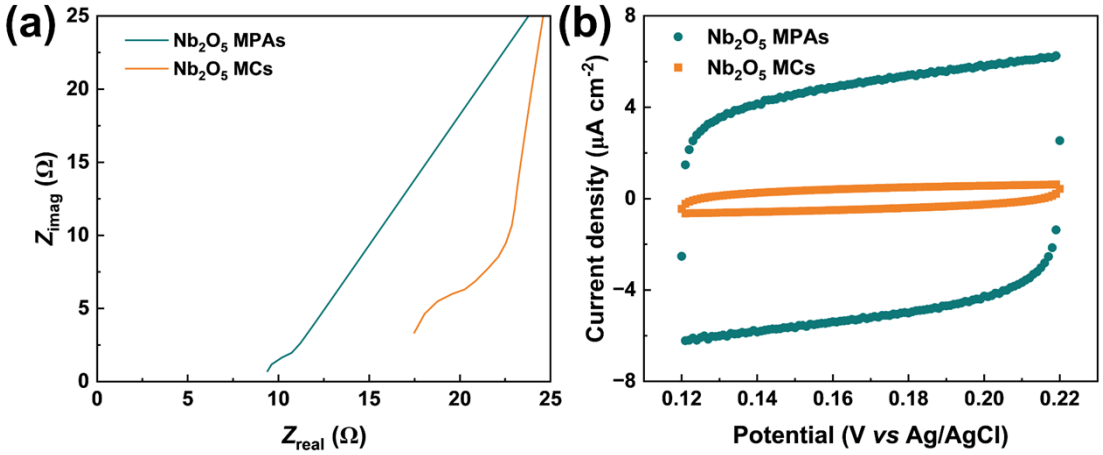

Figure S7. a) EIS curves and b) CV curves of Nb_2O_5 MPAs and MCs.

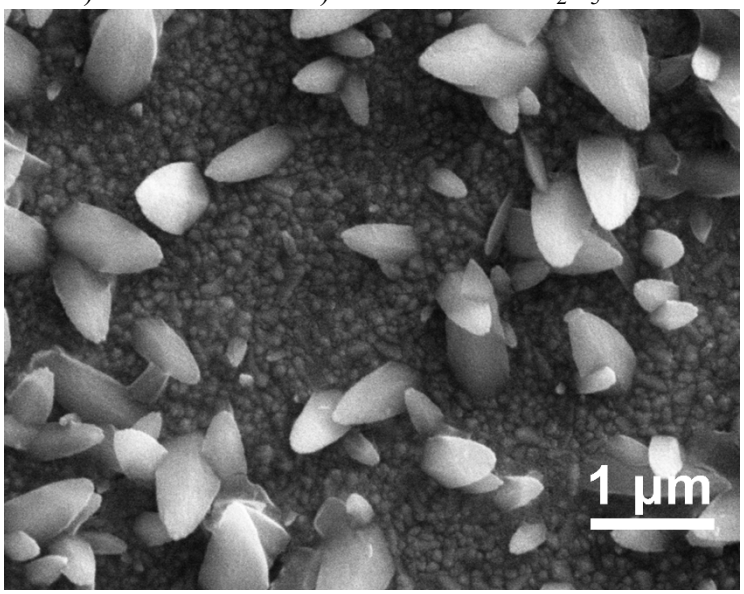

Figure S8. SEM image of the long-term Nb_2O_5 MPA sample.

Table S1. The *P* for 254 nm and 365 nm wavelength of light.

P_λ (μW cm^{-2})	I	II	III	IV	V
254 nm	19.9	39.8	71.6	118	250
365 nm	4600				

Table S2. The J_{ph} of Nb_2O_5 MPA PEC SBUV PDs under 254 nm irradiation with different power intensities.

J_{ph} (μA cm^{-2}) / Sample	I	II	III	IV	V
1 h	0.5673	0.7459	0.9097	1.2867	2.6909

2 h	2.9141	3.6789	5.1856	7.3747	13.7340
3 h	0.7413	0.9582	1.3541	2.1949	3.9415

Table S3 The *R* of Nb_2O_5 MPA PEC SBUV PDs under 254 nm irradiation with different power intensities.

Sample \ *R* (mA W^{-1})	I	II	III	IV	V
1 h	28.5075	18.7412	12.7053	10.9042	10.7636
2 h	146.4372	92.4347	72.4246	62.4975	54.9356
3 h	37.2513	24.0704	18.9106	18.6008	15.76

Table S4. Comparison table with other PEC PDs.

Materials	Wavelength (nm)	Power intensity (μW cm^{-2})	Rejection ratio	Bias (V)	*R* (mA W^{-1})	Electrolyte	t_r (ms)	t_f (ms)	Ref.
Nb_2O_5 MPAs	254	19.9	22306(254/365)	0	146.44	Seawater	80	90	Ours
α-Ga_2O_3	254	79	126.4(254/365)	0	101.5	0.01 M Na_2SO_4	1000	5000	1
β-Ga_2O_3	213	318	N/A	0	1.51	Seawater	220	140	2
α-Ga_2O_3/CFP	254	100	N/A	0	12.9	0.5 M Na_2SO_4	150	130	3
Ga_2O_3/Al_2O_3	254	2000	34.8 (264/400)	0	12.45	0.1 M NaOH	100	100	4
Ga_2O_3/ZnO	266	127000	N/A	0	7.97	0.5 M Na_2SO_4	150	1100	5
In_2O_3	254	39	1319(254/365)	0	86.15	1 M KOH	15	18	6
In_2O_3	254	40	1567(254/455)	0.4	172.36	0.5 M Na_2SO_4	800	2200	7
Ga-In	254	79	262.45(254/455)	0	50.04	0.01 M Na_2SO_4	450	380	8
ZnAl-LDH	254	40	1037(254/455)	0	29.25	0.01 M KOH	100	100	9
SnO_2	254	40	158.73(254/365)	0	68.08	1 M Na_2SO_4	60	60	10
ZnS NPF	254	40	1343(254/455)	0	241.74	0.01 M Na_2SO_4	15	15	11
AlGaN/GaN	254	100	N/A	0	20.9	Seawater	121	151	12
AlGaN: Ru	254	1500	N/A	0	48.8	0.01 M H_2SO_4	83	19	13

Table S5. The *D** of Nb_2O_5 MPA PEC SBUV PDs under 254 nm irradiation with different power intensities.

Sample \ *D**(10^{10} Jones)	I	II	III	IV	V
1 h	2.8172	1.9799	1.3669	1.1603	1.1474
2 h	17.4527	10.5476	8.3517	6.7996	6.3896
3 h	3.9354	2.4549	1.9631	1.7501	1.6417

Table S6. The calculated I_{ph}, R and D^* values of 2 h-Nb_2O_5 PEC PDs illuminated by 365 nm at level I in simulated seawater and Nb_2O_5 MCs PEC SBUV PDs for 254 nm light at level I in simulated seawater, respectively.

Parameter / Irradiation	J_{ph} (μA cm^{-2})	R (mA W^{-1})	D^* (10^{10} Jones)
2 h (365 nm, I)	0.0302	0.006565	0.027115
MCs (254 nm, I)	0.1165	5.855	0.3517

Table S7. The fitted R_s and R_{ct} of Nb_2O_5 MPA PEC SBUV PDs and MC PEC PDs.

Sample / Sample	1 h	2 h	3 h	MCs
R_s	10.27	8.97	9.819	14.48
R_{ct}	13.41	8.1	12.85	29.17

Ref.

(1) Qu, L.; Ji, J.; Liu, X.; Shao, Z.; Cui, M.; Zhang, Y.; Fu, Z.; Huang, Y.; Yang, G.; Feng, W. Oxygen-vacancy-dependent high-performancealpha-Ga_2O_3 nanorods photoelectrochemical deep UV photodetectors. *Nanotechnology* **2023**, *34* (22), 225203. DOI: 10.1088/1361-6528/acbfbd.

(2) Zhang, N.; Lin, Z.; Wang, Z.; Zhu, S.; Chen, D.; Qi, H.; Zheng, W. Under-Seawater Immersion beta-Ga_2O_3 Solar-Blind Ultraviolet Imaging Photodetector with High Photo-to-Dark Current Ratio and Fast Response. *ACS Nano* **2024**, *18* (1), 652-661. DOI: 10.1021/acsnano.3c08814.

(3) Huang, L.; Hu, Z.; Zhang, H.; Xiong, Y.; Fan, S.; Kong, C.; Li, W.; Ye, L.; Li, H. A simple, repeatable and highly stable self-powered solar-blind photoelectrochemical-type photodetector using amorphous Ga2O3 films grown on 3D carbon fiber paper. *Journal of Materials Chemistry C* **2021**, *9* (32), 10354-10360. DOI: 10.1039/d1tc02471j.

(4) Zhang, J.; Jiao, S.; Wang, D.; Gao, S.; Wang, J.; Zhao, L. Nano tree-like branched structure with α-Ga_2O_3 covered by γ-Al_2O_3 for highly efficient detection of solar-blind ultraviolet light using self-powered photoelectrochemical method. *Applied Surface Science* **2021**, *541*, 148380. DOI: 10.1016/j.apsusc.2020.148380.

(5) Ni, D.; Wang, Y.; Li, A.; Huang, L.; Tang, H.; Liu, B.; Cheng, C. ALD oxygen vacancy-rich amorphous Ga_2O_3 on three-dimensional urchin-like ZnO arrays for high-performance self-powered solar-blind photodetectors. *Nanoscale* **2022**, *14* (8), 3159-3165. DOI: 10.1039/d1nr08262k.

(6) Zhang, N.; Gao, X.; Guan, H.; Sun, S.; Liu, J.; Shao, Z.; Gao, Q.; Zhang, Y.; Sun, R.; Yang, G.; et al. Three-dimensional porous In_2O_3 arrays for self-powered transparent solar-blind photodetectors with high responsivity and excellent spectral selectivity. *Nano Research* **2023**, *17* (5), 4471-4477. DOI: 10.1007/s12274-023-6370-y.

(7) Zhang, M.; Yu, H.; Li, H.; Jiang, Y.; Qu, L.; Wang, Y.; Gao, F.; Feng, W. Ultrathin In_2O_3 Nanosheets toward High Responsivity and Rejection Ratio Visible-Blind UV Photodetection. *Small* **2023**, *19* (1), 2205623. DOI: 10.1002/smll.202205623.
(8) Shao, Z.; Qu, L.; Cui, M.; Yao, J.; Gao, F.; Feng, W.; Lu, H. Achieving High-Performance Self-Powered Visible-Blind Ultraviolet Photodetection Using Alloy Engineering. *ACS Appl Mater Interfaces* **2023**, *15* (37), 43994-44000. DOI: 10.1021/acsami.3c08077.
(9) Sun, S.; Zhang, Y.; Gao, Q.; Zhang, N.; Hu, P.; Feng, W. ZnAl-LDH film for self-powered ultraviolet photodetection. *Nano Materials Science* **2024**. DOI: 10.1016/j.nanoms.2024.05.001.
(10) Yu, H.; Qu, L.; Zhang, M.; Wang, Y.; Lou, C.; Xu, Y.; Cui, M.; Shao, Z.; Liu, X.; Hu, P.; et al. Achieving High Responsivity of Photoelectrochemical Solar-Blind Ultraviolet Photodetectors via Oxygen Vacancy Engineering. *Advanced Optical Materials* **2022**, *11* (4), 2202341. DOI: 10.1002/adom.202202341.
(11) Zhang, Y.; Shao, Z.; Zhou, J.; Sun, S.; Sun, R.; Zhang, N.; Liu, J.; Gao, X.; Hu, P.; Feng, W. Vacancy Engineering Optimizing Solid/Liquid Interfacial Properties for Boosting Self-Powered Solar-Blind Photodetection. *Advanced Optical Materials* **2024**, *12* (34), 2401639.DOI: 10.1002/adom.202401639.
(12) Luo, Y.; Wang, D.; Kang, Y.; Liu, X.; Fang, S.; Memon, M. H.; Yu, H.; Zhang, H.; Luo, D.; Sun, X.; et al. Demonstration of Photoelectrochemical-Type Photodetectors Using Seawater as Electrolyte for Portable and Wireless Optical Communication. *Advanced Optical Materials* **2022**, *10* (10), 2102839. DOI: 10.1002/adom.202102839.
(13) Wang, D.; Huang, C.; Liu, X.; Zhang, H.; Yu, H.; Fang, S.; Ooi, B. S.; Mi, Z.; He, J. H.; Sun, H. Highly Uniform, Self-Assembled AlGaN Nanowires for Self-Powered Solar-Blind Photodetector with Fast-Response Speed and High Responsivity. *Advanced Optical Materials* **2020**, *9* (4), 2000893. DOI: 10.1002/adom.202000893.